Molecular Crystals and Liquid Crystals Science and Technology. Section A. Molecular Crystals and Liquid Crystals

Publication details, including instructions for authors and subscription information:
http://www.tandfonline.com/loi/gmcl19

Accelerated Mineralization of Prosthetic Heart Valves

Michael D. Banas [a] & Robert E. Baier [a]

[a] State University of New York at Buffalo, Industry/University Cooperative Research Center for Biosurfaces, Buffalo, NY, 14214-3007, USA

Version of record first published: 24 Sep 2006

To cite this article: Michael D. Banas & Robert E. Baier (2000): Accelerated Mineralization of Prosthetic Heart Valves, Molecular Crystals and Liquid Crystals Science and Technology. Section A. Molecular Crystals and Liquid Crystals, 354:1, 249-267

To link to this article: http://dx.doi.org/10.1080/10587250008023619

Mol. Cryst. and Liq. Cryst., 2000, Vol. 354, pp. 249-267
Reprints available directly from the publisher
Photocopying permitted by license only

Accelerated Mineralization of Prosthetic Heart Valves

MICHAEL D. BANAS and ROBERT E. BAIER

State University of New York at Buffalo, Industry/University Cooperative Research Center for Biosurfaces, Buffalo, NY 14214–3007, USA

The most common cause of prosthetic heart valve failure is severe regurgitation due to rupture of one or more valve cusps that have become mineralized and rigid. To assess the role of stress and strain in the mineralization initiation, *in vitro,* reference-grade, essentially lipid-free, glutaraldehyde-tanned bovine pericardium (developed as a standard reference material for bioprosthetic device testing) was exposed to a supersaturated calcium phosphate solution in a high-speed valve tester.

The pericardium was tested as sheets constructed into tricuspid valves and dumbbell-shaped tensile-test specimens, and then tested at 720 cycles/min. for up to 18 million cycles. Mineralization was followed using X-ray photography, energy-dispersive X-ray analysis, field-emission scanning electron microscopy, and multiple-attenuated internal reflection infrared spectroscopy. Tensile strength of the tissue was determined using a chemomechanical testing apparatus.

Phosphate-based tissue mineralization, first concentrated superficially in an annular distribution at the valve cusp bases, was followed by minimal diffuse calcification within the valve cusps. Small crystalline patches also appeared in the tissue compressed by the valve support rings. Mineralization occurred in a distribution similar to that found in clinically explanted prosthetic heart valves, in areas of maximal tensile and compressive stress and maximal strain. Infrared and tensile test data combine to show that tissue fatigue due to cyclic loading most likely caused breakage of collagen cross-links. Exposure of superficial broken cross-link sites, and unmasking of hydroxyproline binding sites, of the tissue collagen are thus implicated as the main factors in phosphate-radical nucleation events leading to valve mineralization, overshadowing previously cited contributions from tissue lipids and membranes. Mineralization first occurs at the surface regions subjected to the greatest stress and strain, and begins as amorphous phosphate-rich rather than crystalline calcium-rich deposits.

Keywords: calcification; mineralization; phosphate; tissue; valves; heart; accelerated testing; cyclic; tensile; X-ray; infrared; electron microscopy

INTRODUCTION

The most common cause of prosthetic heart valve failure is severe regurgitation due to a tear or rupture of one or more valve cusps that have become mineralized and rigid.[1,2,3] Some *in vivo* studies have shown that mineralization of bioprosthetic heart valves occurs at points of maximal mechanical deformation [4,5] while others have shown that mineralization occurs at points of increased mechanical stress.[6,7,8]

White[9] developed an *in vitro* model to determine the nature of the mineralization process of bioprosthetic, glutaraldehyde-fixed heart valves, using a supersaturated solution of calcium phosphate in conjunction with a high-speed mechanical valve testing apparatus. Mineralization was examined under physiologic pressures, physiologic flows, and accelerated flexing rates *in vitro*.

Results showed excellent simulation of the *in vivo* observations, with mineral deposition on the inflow sides of the valves primarily at the cuspal commissures and basal attachments.

The goal of this further experimental work was to investigate the mineralization of a reference-grade, glutaraldehyde-tanned bovine pericardium tissue (developed by Columbia Labs, Buffalo, NY) specifically produced as a standard reference material for bioprosthetic device testing. This tissue is very well characterized and is intended to be available commercially to the industrial and scientific communities.

The reference-grade tissue was constructed into tricuspid heart valves and dumbbell shaped specimens to determine the roles of differing degrees of stress and strain on the mineralization initiation. The stresses and strains on the simulated heart valve tissue were determined by stroboscopic photography and engineering analysis. The degree of mineralization was characterized using x-ray photography, energy-dispersive X-ray analysis, field-emission scanning electron microscopy,

and multiple-attenuated-internal-reflection infrared spectroscopy.

MATERIALS AND METHODS

A high-speed valve tester was provided by Columbia Labs, Buffalo, NY, shown in Figures 1 and 2. This device consists of two chambers, A and B, between which test specimens were placed, connected by a compliance chamber. A DC engine with a maximum output of 20 Hz drove a Delrin lever arm and elastic bladder to produce an oscillating flow that flexed the specimens and forced the test valves open and shut.

A supersaturated calcium phosphate solution was used that contained the following ionic concentrations:

Ca^{2+}	4.0 mM	PO_4^{3-}	2.4 mM
Na^{+}	145.0 mM	OH^{-}	19.9 mM

The four natural heart valves are exposed to unidirectional blood flows within the human body. With each beat of the heart, changes in pressure from diastolic to systolic cause the valves to open and close. Our high-speed valve tester simulated this unidirectional flow, and we were able to both control and measure the systolic and diastolic pressures in the device to effectively simulate the conditions existing around the heart valve of a human patient.

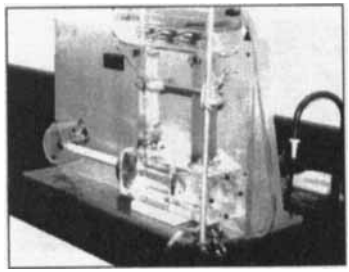

FIGURE 1. High-speed valve tester.

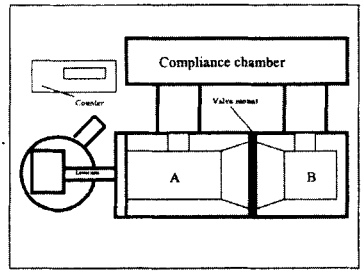

FIGURE 2. Valve tester schematic.

Before each test, the dimensions of each sample of tissue were recorded and X-ray photographs (courtesy of Dr. Lawrence Wolfgang, University at Buffalo) were taken to provide a baseline for later analysis.

For each test, a reference-grade bovine pericardium sample was cut using a plastic template such that a tricuspid valve could be simulated (Figure 3). The simulated tricuspid valve was then placed in the high-speed valve tester and subjected to an oscillating flow of supersaturated solution for a varied number of cycles at an experimental rate.

After each test, the bioprosthetic reference material was examined visually, and then examined using X-ray photography, energy-dispersive X-ray analysis, field-emission scanning electron microscopy, digital subtraction radiography, and multiple-attenuated internal reflection infrared spectroscopy.[10,11] Energy dispersive X-ray analysis provided semi-quantitative analyses of the near-surface elemental compositions of the simulated heart valve tissue to an approximate depth of 50μm. Field emission scanning electron microscopy allowed for high resolution, high-depth-of-field imaging of the simulated heart valve tissue surface regions. Multiple-attenuated-internal-reflection infrared spectroscopy provided a chemical analysis of covalently bound components in the outermost surface zone of the simulated heart valve tissue, to an approximate depth of 0.1μm.

Stress and strain were determined using stroboscopic photography with analytical engineering analysis. Briefly, in this process, a strobe light, set to flash at the same frequency as the flow cycle rate of the high-speed valve tester, was used in conjunction with a camera to take a "still" picture of the flexing, simulated pericardial tissue heart valve. Figures 4 and 5 show a valve being cycled in the high-speed valve tester.

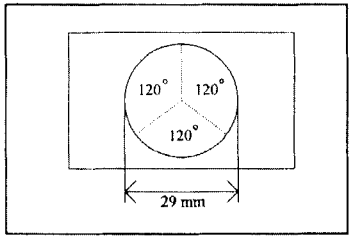

FIGURE 3. Design of simulated valve.

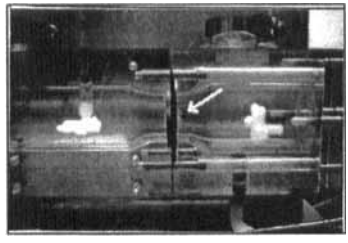

FIGURE 4. Pericardium valve cycling in tester. Arrow points to valve.

The hydraulic pressure exerted on the sample was determined using a column of fluid attached to the front of the high-speed valve tester.

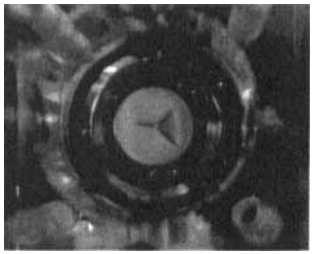

FIGURE 5. Pericardium valve cycling in tester from axial direction.

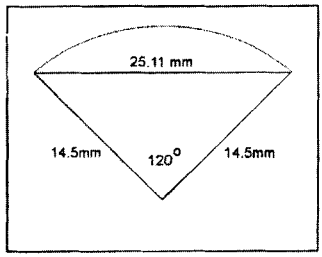

FIGURE 6. Dimensions of valve cusp.

To locate areas of apparent maximal sample stress, we modeled the valve cusp, (Figure 6) as a beam (Figure 7) with a moment of inertia dependent upon the cross-sectional area of the triangular valve cusp.

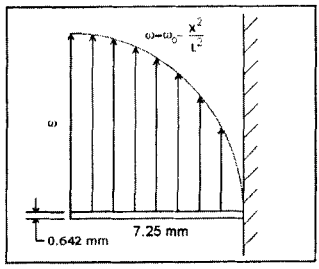

FIGURE 7. Valve cusp modeled as a cantilever beam with a stress distribution ω.

We assumed, as a first approximation, that there was a uniform pressure distribution of the fluid force. The equation for the sample tensile stress became that shown in Equation 1.[12] Here, σ_T is the tensile stress at a given point along the sample, M is the bending moment, c is the distance from the centroid of the cross-section to the point of maximum cross-sectional tensile stress, and I is the moment of inertia. Equation 2 shows the moment M, equal to the force F times the distance d from the point of the bending moment to the site where tensile stress is in question. Equation 3 further relates the force F to the distributed load ω times the length of the distributed load x.

$$\sigma_T = \frac{Mc}{I} \quad (1) \qquad M = Fd \quad (2) \qquad F = \omega x \quad (3)$$

Thus, by substitution Equation 1 became Equation 4.

Since there was a cyclic fluid force on the sample, the distribution of force on the sample became parabolic in shape as shown in Figure 7.[13] The distributed load ω became that derived from Equation 5, where L=7.25mm. Here, ω_0 is the maximal force on the sample (determined from the measured height of the chamber fluid column, converted to Newtons). As a result, Equation 4 became Equation 6 shown below.

$$\sigma_T = \frac{\omega x dc}{I} \qquad (4) \qquad\qquad \omega = \omega_0 - \left(\frac{x^2}{L^2}\right) \qquad (5)$$

Due to the parabolic nature of the distributed force, d was dependent upon x; Equation 7 assumes d is a function of x based on the equation of the centroid of a parabolic spandrel.[12]

$$\sigma_T = \frac{\left(\omega_0 - \left(\frac{x^2}{L^2}\right)\right) x dc}{I} \qquad (6) \qquad\qquad d = \frac{x}{4} \qquad (7)$$

Thus, Equation 6 became Equation 8, the final formula used to estimate the tensile stress along the sample tissue.

We modeled each triangular valve cusp as a beam. Thus, the moment of inertia I had to be determined for a rectangular cross section using Equation 9. The base b of the triangle was dependent upon the location within the cusp where the stress was to be calculated, and h was the valve cusp thickness.

The strain at points along the sample was calculated from Equation 10, where σ was the tensile stress at that point, E is Young's modulus for the reference-grade bovine pericardium, and ε is the strain.[14]

$$\sigma_T = \frac{\left(\omega_0 - \left(\frac{x^2}{L^2}\right)\right) \frac{x^2}{4} c}{I} \qquad (8) \qquad I = \frac{bh^3}{12} \qquad (9) \qquad\qquad \sigma = E\varepsilon \qquad (10)$$

Young's modulus was determined by testing sections of reference-grade bovine pericardium for actual tensile strengths using a tensile testing machine similar to an Instron, provided by Columbia Labs. We used the ASTM standard protocol for tensile properties,[15] testing all samples of reference-grade bovine pericardium first cut as shown in Figure 8.

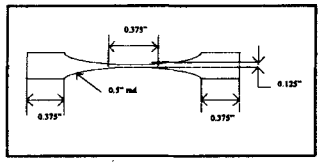

FIGURE 8. Sample dimensions for tensile loading.

Identical testing revealed the effects of mineralization on the tensile strengths of the variously cycled reference-grade pericardium specimens. Control material was not exposed to the cyclic mineralization challenge. Other tissue samples, first cut as shown in Figure 8, were exposed to 4 million cycles at 720 cycles/min. in the high-speed valve tester and then tested for tensile strength. A third sample type was uncut tissue sheet placed in the high-speed tester and also exposed to 4 million cycles at 720 cycles/min. At the end of the test, the sample was cut to shape as shown in Figure 8, and then subjected to tensile testing.

RESULTS

The results of X-ray photography are shown in Figure 9 for a reference-grade bovine pericardium sample subjected to one million flexing cycles in supersaturated calcium phosphate solution over a period of one day at 720 cycles/min. Annular concentration of mineral appeared around the valve perimeter bordered by the valve support rings during testing.

A bovine pericardium sample flexed for 4 million cycles over 4 days at 720 cycles/min., gave the X-ray photographic images shown in Figure 10. This figure also shows an annular distribution of mineral around the valve cusp bases, with diffuse mineralization extending toward the specimen center.

Table 1 summarizes the data used to estimate the stress and strain along the sample tissue using the above method. These data clearly show that the stresses were greatest at the valve cusp bases, and least at the valve cusp tips. Table 1 shows that the strain also was greatest at the valve cusp bases, and least at the tips.

Figures 11 through 14 show the greatest degree of mineralization at the valve cusp bases.

Sample	h cm_{H2O}	ω_o N	L mm	x mm	ω N	B mm	I mm^4	c mm	σ N/mm^2	E N/mm^2	ε %
1 vft	32.5	6.455	7.25	1	6.634	3.462	0.076	0.321	7.005	19.05	36.8
1 vfc	32.5	6.455	7.25	3.5	6.421	12.117	0.267	0.321	23.641	19.05	124.1
1 vcb	32.5	6.455	7.25	7	5.722	24.234	0.534	0.321	42.135	19.05	221.2
2 vft	33.7	6.694	7.25	1	6.675	3.462	0.076	0.321	7.048	19.05	37.0
2 vfc	33.7	6.694	7.25	3.5	6.461	12.117	0.267	0.321	23.789	19.05	124.9
2 vcb	33.7	6.694	7.25	7	5.762	24.234	0.534	0.321	42.430	19.05	222.7
3 vft	32.1	6.376	7.25	1	6.357	3.462	0.076	0.321	6.712	19.05	35.2
3 vfc	32.1	6.376	7.25	3.5	6.143	12.117	0.267	0.321	22.618	19.05	118.7
3 vcb	32.1	6.376	7.25	7	5.444	24.234	0.534	0.321	40.088	19.05	210.4

TABLE 1. vft=valve cusp tip, vfc=valve cusp center, vcb=valve cusp base; h=standing H_2O column height; ω_o=ρghA, where ρ=water density=1000kg/m^3; g=9.8m/s^2, A=area; s=beam length along valve cusp (Figure 6); ω=distributed load; x=distributed load length; I=bh^3/12, where h=0.642 (valve cusp thickness) and b is base length of cross sectional area; E=Young's modulus for bovine pericardium.

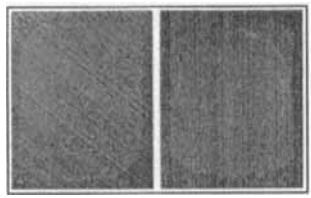

FIGURE 9. X-ray of sample where A shows sample before testing. B shows sample after $1x10^6$ cycles.

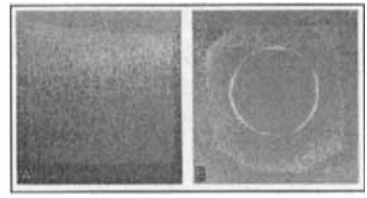

FIGURE 10. X-ray of sample where A shows sample before testing. B shows sample after $4x10^6$ cycles.

Figure 15 is the elemental spectrum associated with the tissue sample depicted in Figure 12 produced through energy-dispersive x-ray analysis.

Figure 15, from the portion of the same sample compressed by the valve rings, showed zinc and chromium peaks resulting from corrosion of the valve mounting rings. Significant new peaks of calcium and phosphate as well as sulfur, chlorine, and sodium appeared as most of the superficial zinc and chromium were eluted away.

Figure 16, taken from the valve cusp, shows significant peaks of calcium and phosphate, as well as sodium, sulfur, and chloride. Figure 17 characterizes a portion of the valve cusp base, which shows its largest peak of phosphorous, and a smaller one for calcium as well as some zinc.

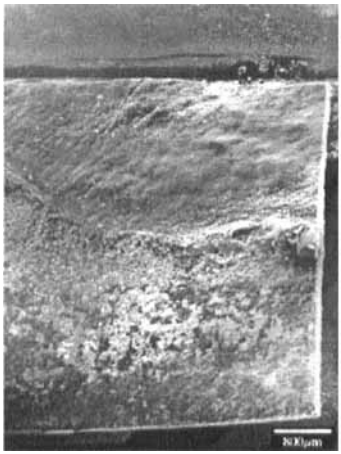

FIGURE 11. Electron microscopy of the sample.

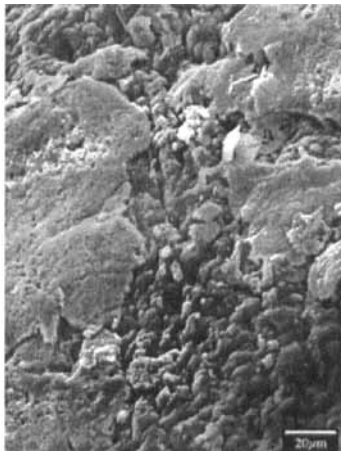

FIGURE 12. Electron microscopy of area compressed by valve support ring.

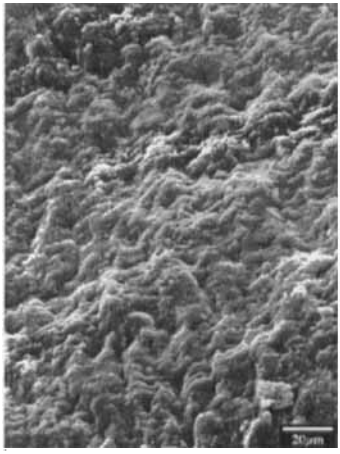

FIGURE 13. Electron microscopy of one of the sample valve cusps.

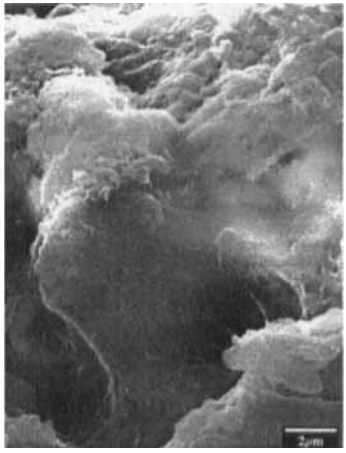

FIGURE 14. Electron microscopy of the cusp base.

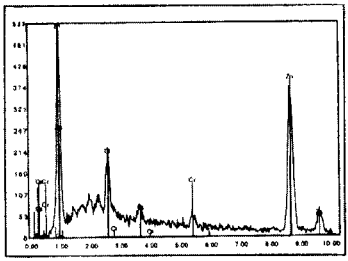

FIGURE 15. Energy-Dispersive X-ray analysis of sample area compressed by valve support rings.

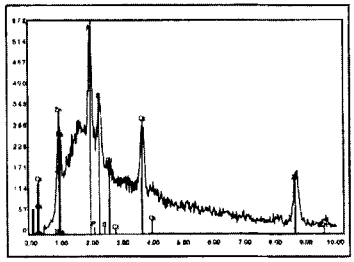

FIGURE 16. Energy-Dispersive X-ray analysis of one of the sample valve cusps.

The results of multiple-attenuated-internal-reflection infrared (IR) spectroscopy for these same specimens are shown below. Figure 18 shows the baseline for the prism used for the bovine pericardium sample. Figure 19 shows the infrared spectrum before any mineralization testing. Figure 20 shows the infrared spectra after drying overnight. In this figure, there are absorption peaks at 1050 cm^{-1} and 1240 cm^{-1} that are of greater amplitude than seen in Figure 19. There also are two common amide peaks, at 1650 cm^{-1} and 1550 cm^{-1}. Many of the peaks produced by infrared spectroscopy are influenced by the degree of sample hydration. However, the amide peak at 1550 cm^{-1} is relatively uninfluenced by hydration. This peak was taken to represent the intrinsic collagen, protein comprising the ultra-structure of the bovine pericardium.

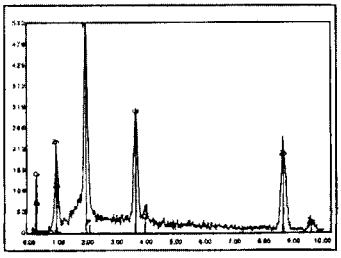

FIGURE 17. Energy-Dispersive X-ray analysis of valve cusp base.

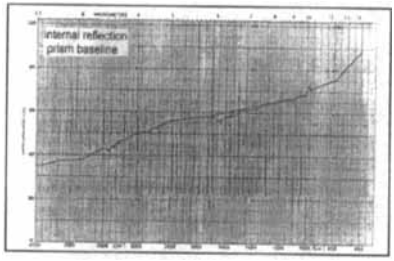

FIGURE 18. Prism baseline for sample.

Thus, we used this peak as a reference to measure the ratio of the mineralization degree to collagen amount in the sample. This ratio also

canceled out the effects of water on the magnitudes of these peaks. This was done for the spectra shown in Figure 19 representing the samples prior to mineralization and Figure 20 representing the samples after cyclic mineralization. The results for three separate samples (Table 2) show that after cyclic flexing, the ratio of mineral to collagen increased for each of the three samples. The increase in this ratio was most likely due to phosphate-OH bonds preceding frank calcium phosphate mineralization. The increased expression of the 1240 cm^{-1} IR absorption after cyclic flexing is taken as evidence that originally H-bonded ring-bound hydroxyls, essentially those abundant as hydroxyproline subunits of the collagen molecules, were re-exposed during mechanical fatigue. These new bonding sites, especially at the margins of physical voids produced as the tissue was increasingly cycled, were the probable niduses for phosphate uptake and mineralization process nucleation.

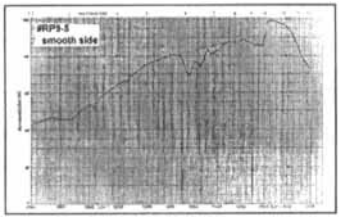

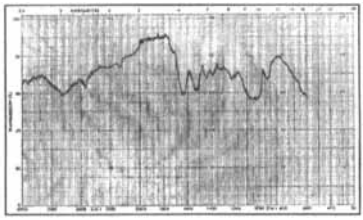

Sample	Area of Mineral peak at 1050 cm^{-1} (mm^2)	Area of Amide peak at 1550 cm^{-1} (mm^2)	Ratio of Mineral to Collagen
1 (prior to mineralization)	11	17	0.647
1 (after mineralization)	24	18	1.333
2 (prior to mineralization)	9	10	0.900
2 (after mineralization)	20	11	1.818
3 (prior to mineralization)	12	12.5	0.960
3 (after mineralization)	39.5	30	1.317

TABLE 2. Ratio of mineral to collagen for Samples 1, 2, and 3.

To determine the degree of progressive mineralization over longer periods of time, samples cycled at 720 cycles/min. were X-ray photographed, still wet, every two million cycles. The results are visually displayed in Figure 21.

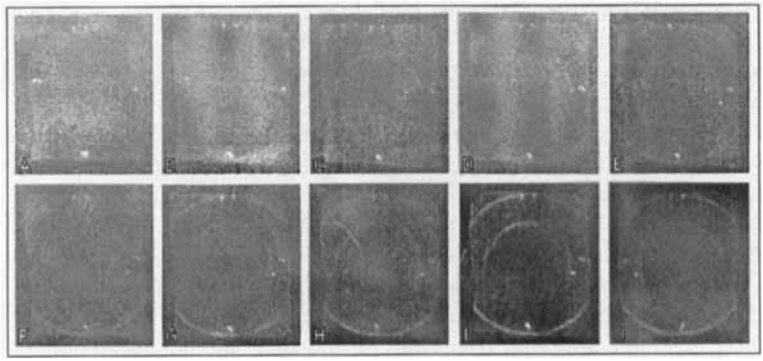

FIGURE 21. A shows sample before testing. B after $2x10^6$ cycles. C after $4x10^6$ cycles. D after $6x10^6$ cycles. E after $8x10^6$ cycles. F after $10x10^6$ cycles. G after $12x10^6$ cycles. H after $14x10^6$ cycles. I after $16x10^6$ cycles. J after $18x10^6$ cycles.

The results clearly show that an increased cycle number promotes an increased degree of mineralization. Combining the infrared data with the x-ray photos, it is found that mineralization begins superficially and then progresses laterally and into the bulk of the samples.

To determine the effect of mineralization on the reference-grade bovine pericardium tensile properties, tissue samples were tested as Control, Dumbbell, and Sheet specimens. The Control sample was not exposed to prior mechanical stress or supersaturated solution. Dumbbell was cut into a dumbbell shape (Figure 8) and placed into the high-speed valve tester and cycled for 4 million cycles at 720 cycles/min. before tensile testing. Sheet, was placed into the valve tester as flat sheet and cycled for 4 million cycles at 720 cycles/min., and then cut into the dumbbell shape before tensile testing. These variations were employed to minimize potential confounding effects from the cut tissue edges.

Stress vs. strain plots for these samples (Figure 22) show Young's moduli of 19.05 N/mm^2, 16.67 N/mm^2, and 10.53 N/mm^2 for Control, Dumbbell and Sheet respectively. Note the differing break strengths of each curve. Dumbbell and Sheet fractured between 4 and 8 MPa after plastic deformation, as opposed to the more elastic Control sample, which sustained over 16 MPa. Thus, the tissue samples exposed to the super-saturated calcium-phosphate solution in the valve tester, were significantly more brittle than the unmineralized Control sample.[16]

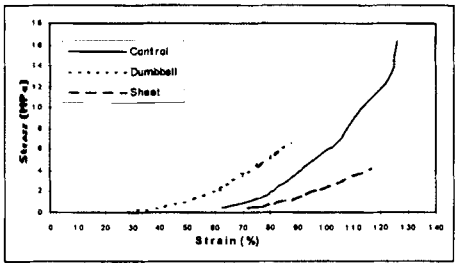

FIGURE 22. Tensile strength of three tissue samples.

Table 3 shows sample dimensions before and after mineralization in the valve tester. For each of the four samples listed, the area increased as the material was cycled demonstrating tissue fatigue caused by cyclic loading, leading to tissue wear and tear by either plastic flow or actual collagen cross-link breakage. The latter circumstance was obtained, at least in part, as indicated by the expression of IR absorptions for newly available hydroxyproline binding sites with increased cyclic flexing.

Zinc and chromium from support washers used to hold the samples of bovine pericardium did leach into the contacting areas of the samples, so caution is exercised in further interpreting these findings.

Sample	Cycles	Height (cm)	Width (cm)	Area (cm^2)
1 (prior to mineralization)	0	4.22	4.30	18.15
1 (after mineralization)	$1x10^6$	4.35	4.40	19.14
2 (prior to mineralization)	0	4.95	4.95	24.50
2 (after mineralization)	$4x10^6$	5.00	4.98	24.90
3 (prior to mineralization)	0	4.90	4.45	21.81
3 (after mineralization)	$4x10^6$	4.95	4.51	22.32
4 (prior to mineralization)	0	4.95	4.15	20.54
4 (after mineralization)	$18x10^6$	5.15	4.30	22.15

TABLE 3. Dimensions for tissue Samples 1, 2, 3, and 4.

DISCUSSION AND CONCLUSIONS

It has been estimated that about one of every hundred of the elderly population has clinically significant aortic stenosis.[17] Much of the data

about the performance of prosthetic tissue heart valves has been obtained from clinical use and *in vivo* animal trials. Gatti et al.[18] tested glutaraldehyde-fixed bovine pericardium heart valves by implanting them in sheep for a period of six months, using X-ray photography to estimate their degree of calcification. Our *in vitro* model was able to assess the degree and nature of calcification in a much shorter period of time, at lower cost, and under more controlled conditions.

No *in vitro* method of testing bioprosthetic heart valve tissue has been developed to produce calcification at both the rate and with morphology similar to *in vivo* models or clinical explants.[19] Our *in vitro* method produces mineralization at as fast a rate as possible with the same pattern of mineralization as that seen in clinically explanted valves.

Bernacca et al.[20] also were able to produce calcification in pericardial valves with similar morphology to that seen in valves explanted clinically. Prosthetic bovine and porcine tissue heart valves have generally been shown to mineralize at the base of the cusps as well as at the cuspal commissures.[21] Interestingly, the most common cause of aortic stenosis of *in situ* human heart valves is degenerative (senile) calcific aortic stenosis.[22] Analyses of clinically explanted aortic heart valves have shown that in degenerative calcific aortic stenosis, deposits of solid amorphous calcium compounds also begin at the base of the cusps where strain is the greatest.[23] Degenerative calcification seen in clinically explanted heart valves rarely involves the free edges of the valve. As a result of increasing deposition of calcium salts, however, valves become stenotic resulting in decreased mobility of the valve cusps. Although most mitral valve stenosis is due to rheumatic fever, some is due to annular calcification of the mitral valve.[24]

Our *in vitro* experiments were able to replicate the mineralization patterns seen in clinically explanted heart valves damaged by degenerative calcification, clearly showing mineralization in an annular pattern at the valve cusp bases with minimal mineralization within the valve cusps themselves.

The reference-grade, glutaraldehyde-tanned bovine pericardium used in these experiments was essentially lipid-free, as determined by prior infrared spectral analyses. It has been generally considered by previous authors [2,25,26] that the lipid fractions of natural tissues, specifically those associated with degrading biomembranes, are implicated in the nucleation of mineral deposits. Our results exclude the possibility of lipids being the main agents involved in the nucleation of mineralization.

Rosanova et al.[27] describe two possible alternative mechanisms for *in vivo* mineralization of heart valves. Their "cellular theory" proposes that mineralization is initiated by cell death which releases lipoproteins, phospholipids, ions, and enzymes to act as sites for mineralization. Their "concentration dependent theory" asserts that mineralization is dependent upon the concentration of minerals in the extracellular fluid. Rosanova et al. implanted diffusion chambers containing bovine pericardium into rabbits fed either a normal diet (control), a diet rich in $CaCl_2$, or a diet rich in vitamin D. They found that the added $CaCl_2$ and more so, the vitamin D, increased the concentrations of calcium in the extracellular fluids of these animals, leading to greater mineralization of the bovine pericardium samples in the diffusion chambers. Thus, they concluded that the humoral concentrations of calcium and vitamin D were important factors in the mineralization of heart valve tissue.

Others [28] have concluded that plasma proteins impregnated in bioprosthetic tissue valves promote pathological changes, since these tissues are devoid of calcification inhibitors, leading to mineralization. Yet others [29] have found that thrombi formed on the surfaces of bioprosthetic tissue valves can lead to mineralization. Since our experiments used a reference-grade, glutaraldehyde-tanned pericardium devoid of living cellular contents, their active products, such as enzymes, phospholipids, plasma proteins and clotting factors are also excluded as major factors for mineralization initiation in our system.

We conclude that cyclic loading leads to structural fatigue damage to the protein structure of the tissue, opening physical and reactive void sites for phosphate-initiated mineralization. Indeed, White[9] found that mineralization was strongly dependent upon both cycle rate and number. This prior work used commercial pericardial patch materials containing abundant lipid material, and showed that with an increase in cycle rate, more lipid was released to the surface of the tested tissue materials. Thus, it was speculated that it was this lipid material which acted as the trigger for crystallization of calcium phosphate minerals. However, our more recent experiments with the identical test system were able to replicate the same mineralization amount and pattern with a reference-grade tissue that was free of lipid. It is more likely that structural defects produced by high degrees of stress and strain during rapid mechanical cycling lead to collagen-based-tissue mineralization, than do any particular released chemicals. The majority of mineralization occurs in that part of the collagenous tissue exposed to the highest stresses and strains.

These high stresses and strains, combined with rapid cyclic loading, likely induce fatigue wear of the prosthetic tissue that includes collagen cross-link breakage. This is consistent with subsequent increases in the material size, as evidenced by our measured increase in tissue sample surface area. It is also likely that the dynamics of producing specimen voids, particularly at their surfaces, are associated with transient production of surface reactive sites that are quickly quenched if soluble phosphate is not present to bind immediately.

Mako et al. [19] tested damaged collagen porcine aortic valve leaflets by implanting them subcutaneously in mice. When compared with an undamaged control sample, no statistical differences were found in the degrees of mineralization. Subcutaneous implantation does not provide the fluidic stresses found in the pulsatile circulation. No dynamic fatigue correlates with no transient reactivity (in spite of subsequent collagen fiber damage), and no increase in mineralization.

This "fatigue-to-damage + reaction" path is likely the route of mineralization within the human patient as well. Clark et al.[30] performed *in vitro* experiments on a number of bioprosthetic and biomechanical heart valves and found that sites of *in vitro* fatigue were identical to sites of clinical *in vivo* fatigue.

A human heart beating at a rate of 72 beats/min. is exposed to 37.8 million cycles/year. Others have attempted to accelerate these condition parameters *in vitro*. Bernacca et al.[20] used an *in vitro* test system at 12 cycles per second in a period of 43 to 145 days. From this work, Bernacca et al. and others [29] also suggested that calcium deposition occurs in the damaged collagen fibrils of fatigued heart valve tissue.

Clark et al.[31] found severe fatigue damage to porcine heart valves tested *in vitro*. They found small tears and holes in the collagen structure at the base of the valve leaflets at 7 million cycles and complete valvular insufficiency at 77 million cycles.

Deiwick et al.[32] used an accelerated *in vitro* test system for bioprosthetic heart valves using a synthetic calcium phosphate solution that simulated the concentrations found in blood plasma. Deiwick et al. used only radiography to characterize the mineralization of the heart valves. They hypothesized that preimplantation processing leads to surface irregularities that cause mineralization, [32] but our reference-grade bovine pericardium was beneficially free of such irregularities.

An intriguing possibility for pathological mineralization of *in vivo* bioprosthetic heart valve tissue is that the high stresses, which we have

confirmed to be located near the base of each of our simulated valve cusps, may also be generated in that part of the existing human arteries and heart tissue to which the prosthetic valve is attached.

Noncollagenous matrix proteins, also may induce valvular calcification. O'Brien et al.[33] hypothesize that mineralization of human heart valves may be an active process where inflammation leads to the production of the protein osteopontin (by macrophages) which thus induces mineralization. Strivasta et al.[34] found that not only osteopontin, but also osteonectin and osteocalcin may promote mineralization. However, since our reference-grade bovine pericardium is basically a dead tanned tissue, this possibility seems unlikely for bioprosthetic heart valves. Nevertheless, production of these proteins may occur in the heart tissue to which the valve is attached.

Watson et al.[35] hypothesized that TGF-β_1 and 25-hydroxycholesterol produced by tissue inflammation can stimulate osteoblast-like vascular cells to calcify. Thus, it may be a combination of fatigue as well as inflammation, which leads to clinical mineralization.

Our combined infrared and x-ray studies determined the degree of superficial versus bulk mineralization of each tissue sample. As the number of cycles to which the tissue was exposed increased, the local density of the mineralization increased as well, indicating that internal calcification of the reference-grade pericardium tissue did occur, (the main phenomenon observed by others).[19]

Observation that the bulk of our tissue samples could mineralize as well as (but after) the surface, supports prior conclusions that fracture failure of prosthetic tissue heart valves is most likely due to mineralization of the bulk of the tissue. Brittle fracture of the prosthetic tissue was evidenced in our tensile testing experiments. This fracture is most likely to occur near the attachment points of the valve to the heart tissue where we showed stress and strain to be the highest.

Smith et al.[36] have proposed that small changes in 3D geometry of porcine bioprosthetic heart valves can induce alterations in the stress distribution along the valve cusp independent of mechanical properties of the tissue and fiber architecture synthetic polymers do mineralize similarly.[37]

Other authors have tried using sodium dodecyl sulfate [29, 38], covalently binding protamine sulfate [39], cross-linking collagen with acyl azide [40], 2-amino oleic acid [41], and ethanol preincubation [26] in an effort to reduce or prevent bioprosthetic heart valve mineralization. Our

apparatus could be used to determine the effects of these modifications on valve failure.

Ongoing experiments should allow us to determine whether modification of cellular infiltration or cellular expression of matrix proteins that regulate mineralization can offer effective therapeutic approaches to the prevention of valve failure secondary to calcification. Our preliminary data suggest that the hyaluronic-acid rich Wharton's gel components of umbilical cord vein grafts may offer this protection against mineralization of bioprosthetic tissue devices.

Acknowledgments

The authors thank Mr. Mark Lauren for the use of his accelerated testing equipment, provision of the reference-grade, glutaraldehyde-tanned pericardium, and experimental guidance. Robert Forsberg provided laboratory assistance, Dr. Lawrence Wolfgang and Linda Read offered use of their X-ray equipment, Mr. Peter Bush allowed use of his electron microscope, EDX, and computer equipment, and Charles Lau allowed use of his computer equipment. All are warmly appreciated.

References

[1] W. Vongpatanasin, L. Hillis, R. Lange, *NEJM,* **335,** 407–416, (1996).
[2] G. Golomb, I. Lewinstein, V. Ezra, F. Schoen, *Biomaterials,* **13,** 353–357, (1992).
[3] T. Chandy, M. Mohanty, A. John, B. Rao, R. Sivakumar, C. Sharma, M. Valiathan, *Biomaterials,* **17,** 577–585, (1996).
[4] M. Davies M, Pathology of Cardiac Valves, London-Boston, *Butterworth* 1990.
[5] F. Schoen, H. Harasaki, K. Kim, C. Aderson, R. Levy, *J. Biomed. Mater. Res.: Applied Biomaterials,* **22,** 11–36, (1988).
[6] M. Fishbein, S. Gissen, J. Collins, E. Barsamian, L. Cohn, *Am. J. Cardiol.,* **40,**331–337, (1977).
[7] U. Bortolatti, A. Milano, A. Mazzucco, C. Valfre, R. Russo, M. Vakute, L. Schivazappa, G. Thiene, V. Gallucci, *Am. J. Cardiol.,* **50,**1051–1054, (1982).
[8] J. Bronzino, The Biomedical Engineering Handbook, Hartford, *CRC Press,* 1995.
[9] J. White, "Dynamically Induced Mineralization of Bioprosthetic Tissue," *Master's Thesis – SUNY Buffalo,* 1995.
[10] R. Baier, A. Meyer, *Int. J. Oral& Maxilofacial Imp.,* **3,** 9–20, (1988).
[11] N. Harrick, "Internal Reflection Spectroscopy," Interscience Publishers, New York, 1967.
[12] F. Beer, E. Johnson, "Mechanics of Materials," *Second Edition,* McGraw-Hill Inc., New York, 1992.
[13] R. Fox, A. McDonald, "Introduction to Fluid Mechanics," *Fourth Edition,* John Wiley & Sons Inc., New York, 1992.
[14] R. Juvinall, K. Marshek, "Fundamentals of Machine Component Design," *Second Edition,* John Wiley & Sons Inc., New York, 1991.
[15] "Standard Test Method for Tensile Properties of Plastics-Designation D638–91$^{\theta 1}$," *ASTM Standards,* 161–173, 1993.

[16] J. Shackelford, "Introduction to Materials Science for Engineers," *Third Edition,* Macmillan Publishing Company, New York, 1992.

[17] F. Robicsek, N. Harbold, *Am. J. aardiol.,* **60,** 857, (1987).

[18] Gatti A, G. Noera, C. Massini, *Life support Systems,* **3(S1),** 177–180, (1985).

[19] W. Mako, I. *Vesely, J. Heart Valve Dis.,* **6(3)**:316–322, (1997).

[20] G. Bernacca, T. Mackay, D. Wheatley, *J. Heart Valve Dis.,* **1(1),** 115–130, (1992).

[21] R. Levy, F. Schoen, H. Anderson, *Biomaterials,* **12,** 707, (1991).

[22] E. Braunwald, "Heart Disease, A Textbook of Cardiovascular Medicine," *Fifth Edition,* W.B. Saunders Company, Philadelphia, 1997.

[23] W. Frankl, A. Brest, "Valvular Heart Disease: Comprehensive Evaluation and Treatment," *Second Edition,* F.A. Davis Company, Philadelphia, 1993.

[24] R. Lewin, G. Dorros, J. King, *J. Am. Coll. Cardiol.,* **14,** 1210, (1989).

[25] W. Chen, F. Schoen, R. Levy, *Circulation,* **90(1),** 323–329, (1994).

[26] N. Vyavahare, D. Hirsch, E. Lerner, J. Baskin, F. Schoen, R. Bianco, H. Kruth, R. Zand, R. Levy, *Circulation,* **95(2),** 479–488, (1997).

[27] B. Rosanova, B. Mischenko, V. Zaitsev, S. Vasin, V, Sevastianov, *J. Biomed. Mat. Res.,* **25,** 277–280, (1991).

[28] S. Krasovskaya, L. Uzhinova, M. Andrianova, A. Prischenko, M. Livantsov, M. Lomonosov, *Biomaterials,* **12,** 817–820, (1991).

[29] S. Bruck, *Int. J. of Artificial Organs,* **8(2),** 65–68, (1985).

[30] R. Clark, W. Swanson, J. Kardos, R. Hagen, R.Beauchamp, *Ann. of Thoracic Surg.,* **26(4),** 323–335, (1978).

[31] R. Clark, W. Swanson, *J. of Thoracic and Cardiovascular Surgery,* **78(2),** 277–280 (1979).

[32] M. Deiwick, B. Glasmacher, A. Zarubin, H. Reul, A. Geiger, G. VonBally, A. Stargardt, G. Rau H. Scheld, *J. Heart Valve Dis.,* **5(4),** 441–447, (1996).

[33] K. O'Brien, J. Kuusisto, D. Reichenbach, M. Ferguson, C. Giachelli, C. Alpers, C. Otto, *Circulation,* **92(8),** 2163–2168, (1995).

[34] S. Strivasta, P. Harrity, P. Maercklein, L. Kleppe, J. Veinot, W. Edwards, C. Johnson, L. Fitzpatrick, *J. of Clin. Investigation,* **99(5),** 996–1009, (1997).

[35] K. Watson, K. Bostrom, R. Ravindranath, T. Lam, B. Norton, L. Demer, *J. of Clin. Investigation,* **93(5),** 2106–2113 (1994).

[36] D. Smith, M. Sacks, P. Pattany, R. Schroeder *J. Heart Valve Dis.,* **6(4),** 424–432, (1997).

[37] R. Batte, "Evaluation of Specimen Preparation Methods for Calcium Phosphate Deposits on Biomaterials," *Master's Thesis – SUNY Buffalo,* 1996.

[38] D. Hirsch, J. Drader, T. Thomas, F. Schoen, J. Levy, R. Levy, *J. Biomed. Mat. Res.,* **27,** 1477–1484, (1993).

[39] G. Golomb, I. Lewinstein, V. Ezra, F. Schoen, *Biomaterials,* **13(6),** 353–356, (1992).

[40] K. Anselme, H. Petite, D. Herbage, *Matrix,* **12**:264–273, (1992).

[41] W. Chen, F. Schoen, R. Levy, *Circulation,* **90(1),** 323–329, (1994).